CoFe nanodumbbells : synthesis, structure, and magnetic properties

Reference:

Liakakos Nikos, Gatel Christophe, Blon Thomas, Bals Sara, van Tendeloo Gustaaf, et al..- CoFe nanodumbbells : synthesis, structure, and magnetic properties

Nano letters / American Chemical Society - ISSN 1530-6984 - 14:5(2014), p. 2747-2754

DOI: http://dx.doi.org/doi:10.1021/nl500734k

Handle: http://hdl.handle.net/10067/1169530151162165141

Co-Fe Nano-dumbbells: Synthesis, Structure and Magnetic Properties.

Nikos Liakakos,[1,2] Christophe Gatel,[2] Thomas Blon,[1] Thomas Altantzis,[3] Sergio Lentijo-Mozo,[1] Cécile Garcia Marcelot, [1] Lise-Marie Lacroix,[1] Marc Respaud,[1] Sara Bals,[3] Gustaaf Van Tendeloo,[3] and Katerina Soulantica[1]*

[1] Université de Toulouse; INSA, UPS, LPCNO, CNRS-UMR5215, 135 avenue de Rangueil, 31077 Toulouse, France

[2] Centre d'Elaboration de Matériaux et d'Etudes Structurales (CNRS), 29, rue Jeanne Marvig, 31055 Toulouse, France

[3] Electron Microscopy for Materials Research (EMAT), University of Antwerp, Groenenborgerlaan 171, 2020 Antwerp, Belgium

ABSTRACT: We report the solution phase synthesis, the structural analysis and the magnetic properties of hybrid nano-structures combining two magnetic metals. These nano-objects are characterized by a remarkable shape, combining Fe nanocubes on Co nanorods. The topological composition, the orientation relationship and the growth steps have been studied by advanced electron microscopy techniques, such as HRTEM, electron tomography and state-of-the-art 3-dimensional elemental mapping by EDX tomography. The soft iron nanocubes behave as easy

nucleation centers that induce the magnetization reversal of the entire nano-hybrid, leading to a drastic modification of the overall effective magnetic anisotropy.

KEYWORDS: metal heterostructures, nanodumbbells, magnetic nanocrystals, epitaxial growth, cobalt, iron

Major advances in the synthesis of nano-crystals by colloidal routes have contributed to the development of a class of complex nanoparticles that combine several materials in the same entity. The co-existence of different materials on the same nano-object increases its functionalities since the individual properties of each component can be present on a single nanoparticle, and even more interestingly opens the way to the discovery of new properties stemming from an interaction between the different materials.[1-5] These possibilities can be exploited towards new applications as well as for fundamental studies. During the last decade, a multitude of inorganic hetero-structured nano-objects, combining completely different materials, have been synthesized.[6-8] Core-shell [9] and asymmetric hetero-structures [10] are two main topologically different classes of multicomponent nanoparticles. Asymmetric hetero-structures, in which the chemically different domains are phase segregated in a non-concentric configuration, offer some additional possibilities such as independent tuning of the size of each domain,[11] or their selective functionalization exploiting their different chemical reactivity.[12]

The seeded growth approach has been widely exploited for the overgrowth of a material on preformed seeds in a topologically controlled fashion.[13] In this respect, anisotropically shaped nanocrystals such as nanorods or tetrapods are ideal seed candidates. Indeed, the different

reactivity along crystallographically distinct facets of anisotropic nanocrystals allows the topologically controlled overgrowth of a different material. The majority of the hetero-structures including an anisotropic section concern semiconductors.[14-17] However, there are fewer reports on hetero-structures comprising metallic rod-shaped nanocrystals.[18-21]

Ferromagnetic, purely metallic Co nanorods [22, 23] combining a high magnetic anisotropy with a high magnetization[24] have been used as seeds for the overgrowth of Au, resulting in the synthesis of Co-Au heterostructures in which epitaxial growth of Au on Co has been achieved.[25] Conversely, Co nanorods have been also grown epitaxially on CdSe nanorods.[26] Epitaxial growth results in crystallographically controlled interfaces, which are of high interest from a fundamental point of view because their investigation enables a better understanding of the interaction between the materials.[27] Preliminary studies concerning the magnetic properties of the above mentioned hybrids have shown that the presence of the second material does not affect the Co magnetic properties. It is therefore of great interest to modulate the magnetic properties of Co nanorods by associating them with another magnetic material. For instance under certain conditions the addition of a high saturation magnetization material like Fe on Co nanorods may increase the energy product and thus enable low-cost permanent magnets compared to rare earth based counterparts.[28-31] In parallel and independently of the magnetic properties, Co-Fe bimetallic nanocrystals could also yield interesting model catalysts for industrially important reactions such as the low temperature Fischer-Tropsch Synthesis.[32, 33]

Here we present the synthesis, the structural analysis and the magnetic properties of Co-Fe hetero-structured nanocrystals taking advantage of our earlier experience in the synthesis of purely metallic Co nanorods [23] and Fe nanocrystals.[34] The Co-Fe nanostructures are characterized using different Transmission Electron Microscopy (TEM) techniques. The growth of Fe on Co nanorods is monitored by High Resolution Transmission Electron Microscopy (HRTEM). Since

conventional TEM images only present a 2D projection of a 3D object, we applied electron tomography to investigate the 3D structure of the nanocrystals.[35-38]The magnetic properties of the hybrid nanocrystals have been measured by SQuID (Superconducting Quantum interference Device) magnetometry.

Bare metallic cobalt nanorods of 77 nm mean length and a mean diameter of 5.5 nm have been prepared by a slight modification of an already published method [23] (see Supporting Information for further details). They are oxide-free hexagonal close packed (hcp) single crystals with their long axis corresponding to the c axis of the hcp structure. They present a ferromagnetic behavior at room temperature with a M_S corresponding to the Co bulk value and a high coercive field (0.65T at T=300 K) due to their single-crystalline structure. [24] These Co nanorods (Figure S1) have been used as seeds for the subsequent growth of iron as described in the Supporting Information. Briefly, anisole solutions of different concentrations containing $[Fe\{N(SiMe_3)_2\}_2]_2$, lauric acid (LA), and hexadecylamine (HDA) in a ratio Fe/LA/HDA = 1/2/1 were added to a fixed amount of a bare Co nanorod suspension which contained HDA (Co/HDA = 1/3). The Fe/Co ratio was adjusted from 1/1 to 12/1 by varying the Fe concentration while keeping the Co nanorod concentration fixed. The mixture was stirred at 150°C under 3 bars of H_2 during 24 hours. The final suspension was let to decant. The transparent supernatant was removed, and the precipitated solid washed with toluene.

In Figure 1, we present conventional TEM images of washed nanocrystals obtained using four different Fe/Co ratios. For a Fe/Co = 1 ratio, the majority of the nanocrystals appears identical to the starting bare nanorods. However, some of them present a modification at one or both their ends (Fig. 1a). The new nano-objects consist of a nanorod and a section that presents a triangular or square-shaped projection as evidenced by the TEM images. An increase of the Fe/Co ratio to 2 results in the development of nanostructures on both tips, for the majority of the nanorods (Fig.

1b). Further increase of the Fe/Co ratio improves the faceting of the cubic-like extremities and increases their mean size (Fig. 1c). When the Fe/Co ratio is increased to 6 (Fig. 1d), apart from a further increase of the cubic domain dimensions, we can also observe irregularities of the rod diameter. The mean dimensions of the domains of the new dumbbells measured from the TEM images are given in Supporting Information Scheme S1 and Table S1. However, when the Fe/Co ratio is increased to 12, Fe overgrowth is so extended that the nanorods are barely visible (see Fig. S2). The X-Ray Diffraction (XRD) patterns of dried powders of the samples Fe/Co = 2, 4 and 6 present the characteristic peaks of hcp Co and body-centered cubic (bcc) Fe structures (Figure S3). For all of these samples, no nano-objects of different morphology, such as bare nanorods, nanocubes or even spherical nanocrystals, were present either in the supernatant or in the solid. The supernatant transparent solutions contain only scarce dumbbells, identical to the ones found in the precipitates. The absence of free Fe nanoparticles indicates that only heterogeneous growth has taken place.

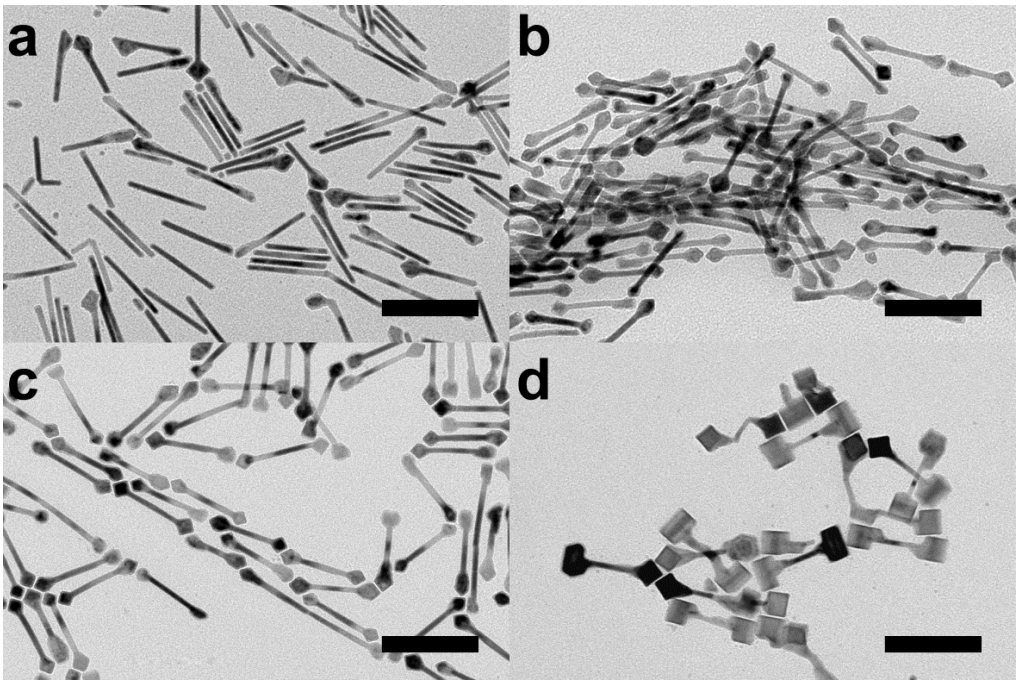

Figure 1. Dumbbells obtained by reaction of different volumes of the iron growth solution to a fixed amount of Co nanorods. (a) Fe/Co = 1. (b) Fe/Co = 2. (c) Fe/Co = 4. (d) Fe/Co = 6. (scale bar = 100 nm).

From the TEM measurements (Table S1) and the Scheme S1 which presents the mean dimensions of the rod and cubic domains for the samples Fe/Co = 2, 4 and 6 we note that the mean length of the apparent nanorod area is shorter than the initial Co seed, indicating either that part of the rod is consumed during Fe growth or that part of the rod is covered by Fe. The rod diameter for Fe/Co = 2 and 4 seems to be slightly larger than the bare nanorod diameter, suggesting a deposition of Fe on the surface of the nanorod.

In order to investigate the structure and composition of the new nano-objects, and to gain better insight into how Fe growth takes place, we applied different TEM techniques. Electron tomography in High Angle Annular Dark Field Scanning Transmission Electron Microscopy (HAADF-STEM) mode has been performed to determine the three-dimensional (3D) morphology of the particles.[39] HAADF-STEM images yield a contrast that scales with the atomic number Z of the elements present in a sample, as well with sample thickness. However, in the present case, the small difference in atomic number Z between Co and Fe does not allow to distinguish between the two components. Therefore, the observed contrast is mainly caused by thickness variations. HAADF-STEM tomography therefore allows investigation of the 3D morphology of the nano-objects.

A tilt series of 2D images was acquired for a single nano-object (Fe/Co = 4/1) over a broad angular range, specified in the Supporting Information. The images were aligned with respect to each other and used as an input for 3D reconstruction. One of the HAADF-STEM images and a

3D visualization of the reconstruction are presented in Figure 2a-c confirming that the Fe domains indeed present a cubic morphology. Both cubes have a diameter close to 20 nm and present a well-defined and regular shape. Note that a curvature appears on those faces of the cube that form the edge which is attached to the Co rod. These concave facets are not an artefact related to the 3D reconstruction. 2D HAADF-STEM (Figure 2d) and TEM images shown in Figure S4 also indicate the presence of cubic tips with concave facets. These concave domains are not systematically present on all nano-objects, but mainly appear on fully-grown cubes of a bigger size. At present their formation and the reason why only two out of the six facets are concave remain unclear.

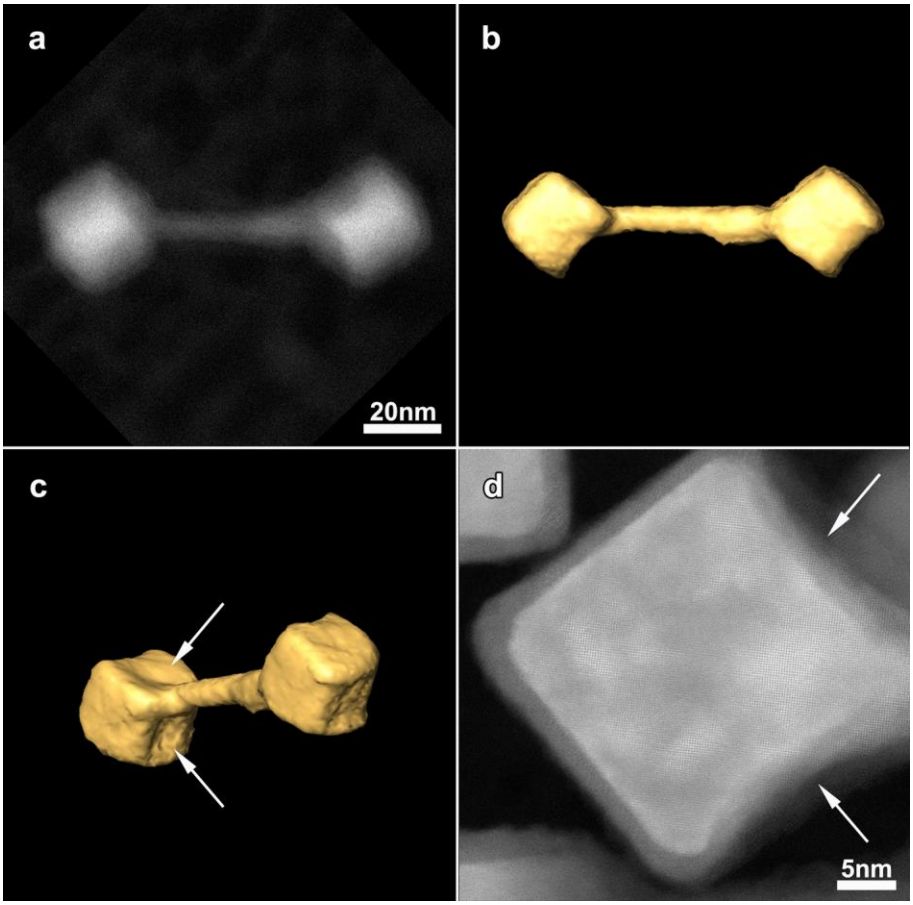

Figure 2. (a) HAADF-STEM image of the dumbbell used for the acquisition of the series. (b) and (c) 3D representation of the reconstructed volume along different viewing directions. We can clearly observe that cubes are attached on both nanorod tips. The facets of the cube that create the edge which is attached to the Co rod, are concave (curvatures are indicated by white arrows). (d) HAADF-STEM image of another particle, focusing on the Fe cube. We can clearly see that the two {100} facets which are connected to the Co rod (indicated by the white arrows), are curved compared to the other two visible {100} facets.

Since Co_xFe_{1-x} alloys can be formed quite easily, we have investigated whether there is a diffusion of Fe into the Co lattice or vice versa. Because of the lack of chemically sensitive contrast in HAADF-STEM mode, we performed Energy Dispersive X-ray (EDX) analysis.

The 2D EDX maps are presented in Figure 3a-c. The EDX tomography is presented in Figure 3d. Such measurements were very challenging until recently because of the inefficiency of the EDX detector and its geometry with respect to the sample.[40] New developments concerning the design of EDX detectors enabled us to combine EDX and electron tomography, leading to a 3D visualization of the chemical structure (Figure 3d). Technical details of this experiment are given in the Supporting Information. A 3D animation of the reconstructed HAADF series together with reconstructed volumes of the Fe and Co EDX maps is also available as Supporting Information.

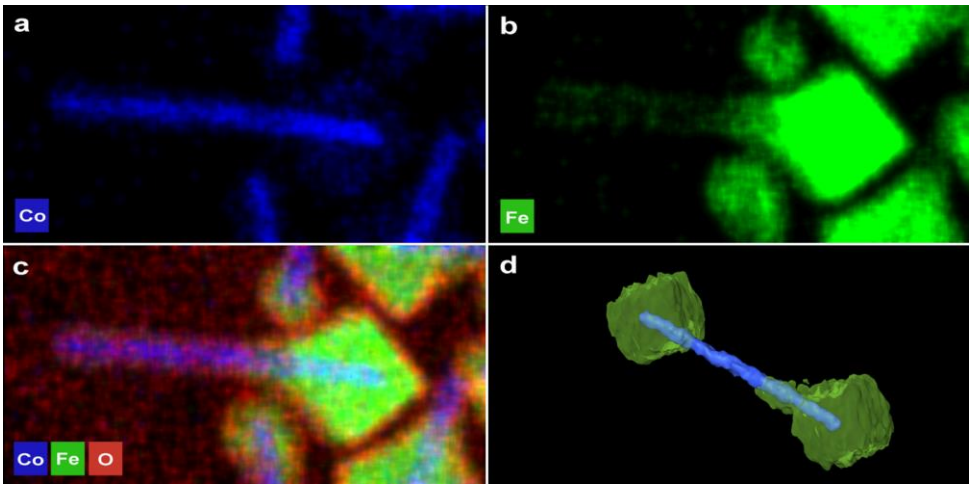

Figure 3. (a), (b) and (c) EDX maps of a group of dumbbells, revealing the distribution of the elements. An O layer is always apparent and its presence is due to the short exposition of the sample to the air (Fe: green, Co: Blue, O: red). (d) 3D representation of the reconstructed volume of the particle shown in Figure 2a-c using EDX tomography, revealing the distribution of the elements. Fe is presented using a transparent visualization in order for the distribution of Fe (green) on the Co rods (blue) to be obvious. We clearly see the segregation between Fe and Co, and the fact that the Co nanorod is encompassed by the Fe cubes.

Two separate domains for Co and Fe have been clearly identified. In addition, we observed that a limited amount of Fe has been deposited on the Co rod close to one of the Fe cubes. The presence of a small amount of Fe on the nanorod has also been detected byElectron Energy Loss Spectroscopy (EELS) measurements presented in the Figure S5. The presence of Fe on the rods may account for the slighter larger diameter of the nanorod domains of Co-Fe dumbbells measured by conventional TEM with respect to the bare Co seeds (Table S1).

In order to investigate in detail the crystal structure of the nano-objects, and obtain information about the interface between the two materials, HRTEM measurements were performed. Figure 4 presents a HRTEM image obtained from a particle obtained with a Fe/Co ratio equal to 1. We clearly see that the hybrid object combines a single-crystalline Co nanorod and a single-crystalline Fe cube grown epitaxially on Co. The cobalt nanorod tips are completely covered by the iron nanostructures . In order to determine the epitaxial relationship between Co and Fe, Fast Fourier Transform (FFT) patterns obtained from selected parts of the particle and from several HRTEM images corresponding to different dumbbells were studied. The FFT patterns presented in the Figure 4 were obtained from the central part and from the outer part of the same dumbbell, indicated by the two white rectangles as Co and Fe respectively. As expected, the growth axis of Co corresponds to the [0001] direction.[22, 23] The zone axis of the Co part corresponds to [2-1-10]. The surfaces enclosing the rod are formed by (01-10) planes (planes parallel to the rod axis). The Fe domains adopt a classical bcc structure and are single crystalline. The zone axis for the Fe part corresponds to [001]. The shape of the Fe nanostructures confirms the one observed by electron tomography and can be well described as a truncated parallelepiped presenting mainly the {100} planes as surfaces with truncated edges exhibiting {110} facets. Considering the 4-fold symmetry of the Fe part, we can establish that {111} planes appear at the corners. Based on these results, a 3D model for the nanostructures is proposed in Figure S6.

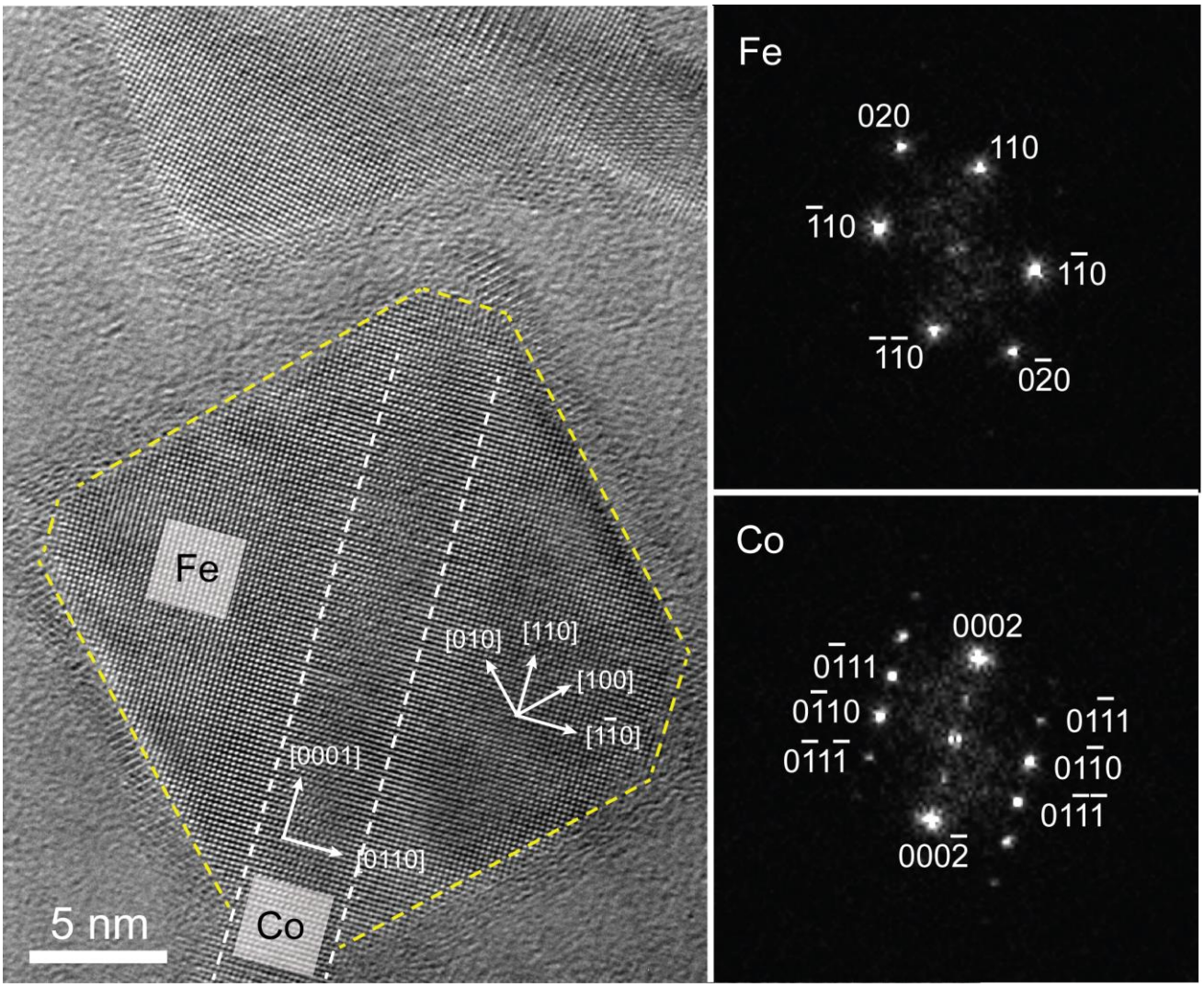

Figure 4. HRTEM micrograph of a Fe-Co dumbbell and FFT patterns obtained from Fe (upper left area) and Co (center lower area) domains of the dumbbell. A shell layer can also be discerned on the surface of Fe domains, composed of oxide due to the exposition of the TEM grid to the air.

Using the FFT patterns extracted from the HRTEM observations we have established different epitaxial relationships between the two domains: (i) Co [2-1-10] (0001) // Fe [001] (110) (planes perpendicular to the rod axis), (ii) Co [2-1-10] (01-10) // Fe [001] (1-10) (planes parallel to the

axis of the rods and to the zone axis of the FFT), (iii) Co [0001] (2-1-10) // Fe [110] (001) (planes parallel to the axis of the rods and perpendicular to the zone axis of the FFT).[41]

The Co-Fe dumbbells seem very similar to some recently reported nano-objects composed of Pt nanocubes exposing {100} facets grown on wurtzite semiconductor nanorods (CdSe@CdS). [42] The fcc structure of Pt presents a preferential alignment of the Pt <110> axis with the <0001> axis of the rod and a misorientation angle of approximately 5°. In our case, Fe and Co domains are linked by a well-defined epitaxial relationship meaning that the dumbbells can be considered as single-crystal structures with the Fe nanocubes surrounding part of the Co nanorod.

From the lattice constants of each domain and for each epitaxial relationship, we calculated the mismatch between the two crystal lattices. These mismatches are presented in Table S2. The mismatch values between the $d_{Co\ 01\text{-}10}$ and $d_{Fe\ 1\text{-}10}$, as well as between the $d_{Co\ 2\text{-}1\text{-}10}$ and $d_{Fe\ 002}$ are quite important and do not allow an epitaxial deformation of Fe with respect to Co. In order to verify this hypothesis some of the HRTEM images have been analyzed by Geometrical Phase Analysis (GPA).[43, 44] The Figure S7 presents the GPA of the strain field of a HRTEM image on a Co-Fe dumbbell (Fe/Co ratio = 1) that corresponds to a nano-object for which Fe growth is not complete. The deformation of the Fe planes parallel to the Co nanorod long axis has been measured to be -6,4% ±0.3 % (reference taken in the Co part) very close to the theoretical mismatch between Co (01-10) and Fe (1-10), indicating that no epitaxial strain occurs and that Fe seems perfectly relaxed on the surface of Co along this direction. Another interesting aspect concerning the relations of the Co (2-1-10) and the Fe (001) planes is their quite important mismatch (-14.3 % with reference to Co). By inversing 0.143 we obtain 6.993, which means that one plane of Fe every seven planes is expected to be in perfect coincidence with a plane of Co. This periodicity type is well known to favor the crystallographic order and thus the epitaxy between different layers.[45]

In order to understand how the growth occurs, we have examined by HRTEM the Fe/Co = 1 sample in which dumbbells at different stages of Fe growth are present after 24h of reaction. In Figure 5 we present micrographs of Fe-Co hybrids at growth stages preceding the almost completely grown nanocube of Figure 4, the less advanced situation shown in Figure 5a and the most advanced in Figure 5c.

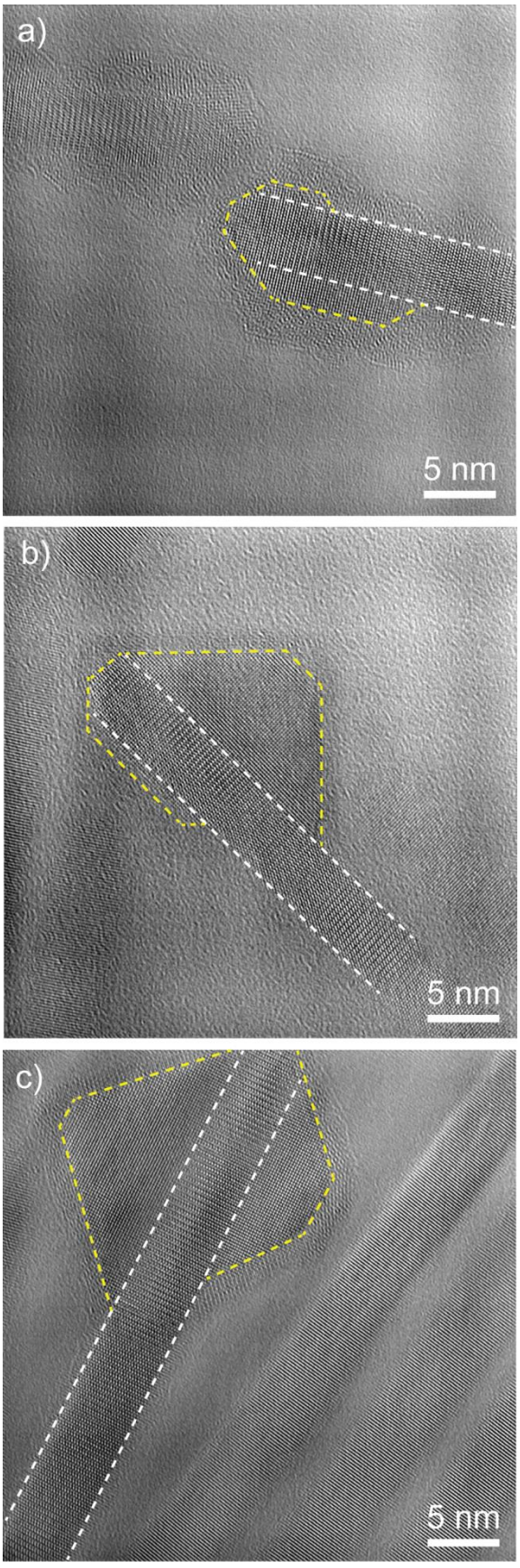
a)
5 nm
b)
5 nm
c)
5 nm

Figure 5. HRTEM micrographs of dumbbells at different growth stages of the Fe/Co =1 sample. (a) initial Fe deposition close to the Co extremity. (b) growth of Fe mainly on one side of the nanorod forming a trigonal prism. (c) the growth of the second prism has started.

The initiation of the growth very close to the tips can be seen in structures in which only a limited amount of Fe is grown (Figure 5a and b). The growth initiation at this location can be explained by the distinct chemical reactivity and surface accessibility along the different nanorod facets. We believe that part of the nanorod tip is less effectively passivated by stabilizing ligands; therefore initial reaction of Fe takes place at these positions. This configuration is not surprising since, as we have previously demonstrated, Au prefers to grow on the extremes of Co nanorods when enough stabilizing ligand is available to cover efficiently the nanorod lateral sides.[25] This is also the case in the present work where the amount of stabilizing LA and HDA is enough to cover efficiently the nanorod lateral sides. Nevertheless, despite the fact that they grow close to the tip, the iron nanocubes have a majority of their contact interfaces with the lateral sides of the nanorods. Indeed, Fe deposition on the lateral sides of Co rods and subsequent growth by formation of (110) facets which grow on the rod lateral facets seems to be favored against the formation of only a small interface on the tip. This diffusion along the nanorod is not extended over the whole nano-rod length and iron growth preferentially continues by addition of atoms on the already deposited iron layers along the nanorod lateral sides. Faceting develops as growth advances. We can distinguish some triangle shaped structures which correspond well to semi-parallelepipeds "cut" through their diagonal (Fig 5b and HAADF-STEM tomography measurements Fig. S8). The appearance of what appear to be two unequal halves of a cube on the same tip (Figure 5c), could be the result either of the growth of

the first half-cube that at a certain moment continues on the periphery of the rod, or the result of a second nucleation event on another point of the tip that starts later. Nanorod tips are not terminated only by clear-cut (0002) facets but may comprise a variable number of higher energy facets. These facets are not always the same on all tips and nucleation may take place at different times depending on their specific reactivity. . Whatever the reason of the appearance of two unequal semi-parallepipedes, finally the Fe domains merge into a single cube, which is the most stable shape under the reaction conditions employed, and the final size of which depends on the Fe/Co ratio (see Table S1). However as can be seen in Figure 3, as well as from the EDX and EELS measurements, Fe can be found also away from the cubic domain towards the center of the nanorod. Taking into account the aspect of Co-Fe hybrids synthesized with a 12/1 Fe/Co ratio (Fig. S2c), it is possible that Fe growth continues along the nanorod at more advanced growth stages and finally completely covers the whole nanorod (Fig. S2).

We believe that during Fe growth, part of the Co is etched away and passes in solution. This has been deduced from the increased Fe/Co ratio in one of the samples (Fe/Co = 4) for which elemental analysis has been performed (Supporting information). Since no free Co nano-objects have been detected in the supernatant, we assume that the missing cobalt corresponds to molecular species or even clusters removed from the sample during washing. It is possible that etching takes place mainly on the nano-rod tips during Fe growth since Co etching from the lateral sides would decrease the rod diameter, which is not in agreement with a slight increase of the mean diameter measured by TEM. Since iron cannot displace cobalt by a galvanic displacement reaction we suggest that some of the laurate ligand liberated in solution from reduced laurate-containing Fe species, interacts with the easily accessible Co atoms close to the tips and etches them away since Co laurate rich species are known to be stable towards reduction.[46]

Both the addition of a different material and the shape modification can modify the magnetic properties of the initial Co nanorods. The bare Co nanorods behave as single domain nanoparticles, with a collinear magnetization. In contrast, Fe is a magnetically "soft" material. For this material, the magnetization behavior is thus mainly dominated by the demagnetizing field and the dipolar interactions between the nano-objects. Thus, Fe nanocubes with size range above 20 nm display a vortex configuration that can be confined within a single isolated nanocube.[47] Moreover, both the morphology of the soft phase on the hard Co nanorod, as well as some inter-diffusion at the two materials interface, may lead to changes. For instance, for a series of $Co_{100-x}Ni_x$ dumbbells, for which upon increasing x, the size of the Ni-rich tips is increased, and at the same time the aspect ratio is reduced, it was observed that the coercive field was lowered.[48] To illustrate these changes, SQuID magnetometry was used in order to measure the magnetic properties of the new hybrid objects obtained with a Fe/Co = 4 ratio. The experimental $M(H)$ hysteresis loops for a powder of bare Co nanorods and a powder of Co-Fe dumbbells measured at 2 K are presented in Figure 6a. For comparison, we also present the hysteresis loop of a powder of Fe nanocubes of 14 nm average size, *i.e.* close to the 16 nm size of the Fe extremities in the Co-Fe dumbbells. The important coercive field of the Co nanorods originates from a high magnetic anisotropy, both due to their elongated shape (shape anisotropy) and to the magnetocrystalline anisotropy of hcp-Co which acts along the hcp-c axis (the long rod axis).

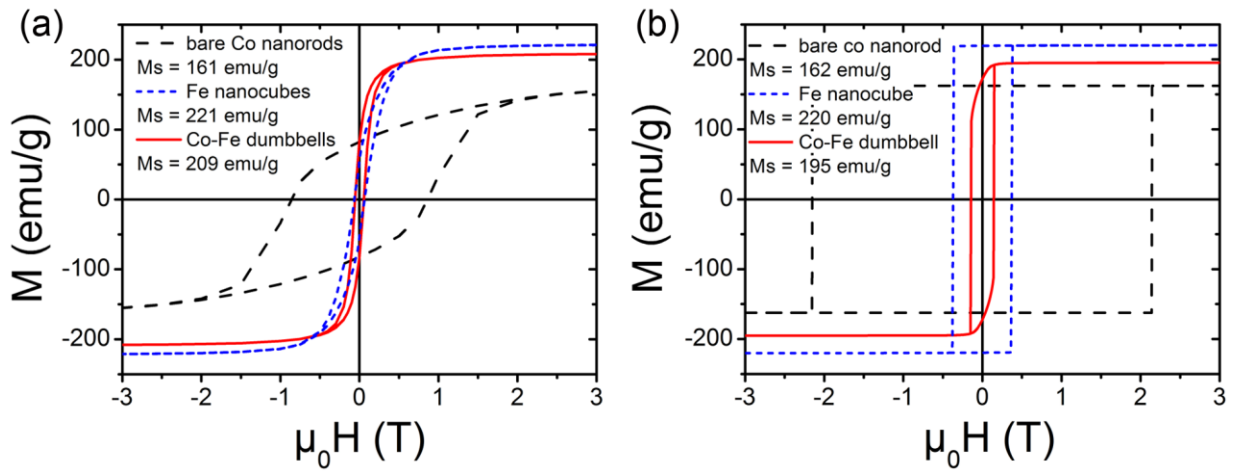

Figure 6. (a) Measured M(H) hysteresis loops at 2 K for bare Co nanorods (black), Fe nanocubes (14 nm) (blue) and Fe-Co dumbbells powders (Fe/Co ratio 4/1) (red). (b) calculated M(H) hysteresis loops along the nanorod axis for a single Co nanorod (black), a single Fe nanocube along the <110> cube direction (blue), and single Co-Fe dumbbell, along the dumbbell long axis (red), using the OOMMF micromagnetic code, 0 K.

The measured hysteresis loop of Co-Fe dumbbells shows a monotonic and continuous reversal of the magnetization with the applied magnetic field, indicating an efficient ferromagnetic exchange coupling between the two phases (Fig. 6a). It has been shown that an effective exchange coupling between hard and soft phases should be achieved if the dimension of the soft phase is smaller than twice the domain wall width of the hard phase, [28-31] this latter being about 16 nm in the present case. In accordance, we show that the exchange coupling is obtained in our case with a soft phase of about 16 nm lateral dimensions, for the Co-Fe dumbbells with a Fe/Co ratio of 4/1 (Fig. 6(a)). Moreover, the soft-hard exchange coupling is expected to be favored by a crystallographic coherence between the two phases,[28,29] as in the present nanocomposite. The initial bare Co nanorods display a saturation magnetization Ms = 161 emu/g very close to the

bulk Co value (162 emu/g). Due to the presence of Fe with a higher magnetic moment than Co, Co-Fe dumbbells present a larger Ms of 209 emu/g. The bare cobalt nanorods exhibit a coercive field of about 0.85 T at 2 K (0.50 T at 300 K, Fig. S9) while for the studied Co-Fe system this value is decreased by a factor 15 to reach 55 mT (36 mT at 300 K, Fig. S9). Note that the coercive fields of the dumbbells are very close to those measured for a powder of Fe nanocubes (65 mT at 2 K (Fig. 6(a)) and 21 mT at 300 K (Fig. S9) of 14 nm average size).[47] Due to higher dipolar effects, the coercive field decreases for bigger Fe nanocubes (32 mT at 2K and 23mT at 300K), of 23 nm average size, which may indicate the key role played by the iron nanocubes.[47,49]

In order to have an insight into the modification of the magnetic properties by the presence of Fe extremities, micromagnetic simulations have been carried out for a single Co nanorod, a single Fe nanocube, and a series of single Co-Fe dumbbells using the 3D version of the OOMMF package.[50] For comparison, the single Fe nanocube hysteresis loop is simulated with an applied magnetic field along the Fe<110> direction because it corresponds to the applied field direction in the Fe extremities for the simulation of the Co-Fe dumbbell. Introducing the dumbbell shapes and dimensions (Table S3) deduced from the TEM analysis and using low temperature bulk magnetic parameters (see Supporting Information), the simulations confirm the ferromagnetic coupling between Fe and Co phases and therefore the increase in saturation magnetization and the decrease of the coercive field (Figure 6b). The slight difference between experimental (209 emu/g) and expected (195 emu/g) saturation magnetizations could be related to the iron nanocube size distribution. The simulations indicate that the coercive field of 2.15 T for a single Co nanorod is decreased by a factor 15 to reach 144 mT due to the presence of Fe extremities, in accordance with the experimental trend. Since Fe is magnetically soft, the magnetization reversal is facilitated. In fact, the Fe extremities behave as centers of nucleation of the magnetization

reversal, transmitted to the Co nanorod core through the ferromagnetic exchange, reducing the coercive field. Indeed, 3D views of the calculated magnetization configurations of a dumbbell at remanence show that the Fe magnetic soft phase allows some spin rotation leading to a better induction closure in and outside the dumbbell in order to decrease the total dipolar energy of the system (Fig. S10). As a consequence, the hybrid Co-Fe nano-objects are softer than the bare Co nanorods, with reduced coercive field and remanence in comparison to the bare Co nanorods, but larger compared to pure Fe nanocubes. This is illustrated by the micromagnetic simulations of dumbbells with different Fe extremity sizes: the larger the Fe extremities, the lower are the coercive field and remanence (Table S4). Finally, for larger Fe extremities, steps characteristic of a multidomain magnetic structure appear in the simulated hysteresis loop (Fig. S11). These trends are driven by the demagnetizing field effect. Moreover, in the measured powder samples, all these effects may be reinforced by the dipolar interaction of the nano-hybrids similarly to a powder of pure Fe nanocubes.[47]

In conclusion, bare cobalt nanorods can serve as seeds for the overgrowth of Fe nanostructures. The epitaxial seeded overgrowth has given rise to hybrids exposing well-defined structural characteristics (facets exposed, shape and size). From the different stages of growth it is deduced that the growth of Fe starts from the tips, continues on the lateral facets along the Co nanorod long axis forming triangular prisms and is completed by the formation of a complete cube surrounding the whole nanorod perimeter. It seems that Co etching from the rod tips is operational during Fe growth whereas a small amount of non-crystallized Fe can be found deposited on the Co domains. The soft anisotropy of the Fe nanocubes and the dipolar magnetic interactions induce a drastic decrease of the magnetic anisotropy of the nano-hybrids, the coercive field of which becomes only slightly higher than the one of interacting Fe nanocubes.

More precise magnetic measurements on isolated nano-hybrids are necessary in order to identify the real magnetization reversal mechanism. By modulation of the Fe/LA/HDA ratio we should be able to induce the shape and size modulation of the Fe domains.[34] Since Co nano-rods of various aspect ratios are available [25] the Co and Fe domain sizes could be independently tailored giving rise to a variety of dumbbells with gradually varied characteristics which could give the opportunity of tuning the magnetic hysteresis loops. The synthesis could be also adjusted in order to yield specimens exposing practically one type of facets for each metal which would be an interesting model catalyst system for syn-gas conversion reactions. Finally, the soft magnetic character that these nanostructures present, should offer the opportunity of heating by application of an externally applied alternate magnetic field during catalysis.[51, 52]

ASSOCIATED CONTENT

Supporting Information. Materials and methods, seed nanorod preparation, dumbbell preparation, dimensions of the Co and Fe domains, TEM of the reaction with a Fe/Co = 12 ratio, XRD patterns of samples with ratios Fe/Co = 2, 4, and 6, TEM of concave cubic domains, EELS, 3D model, mismatch data, GPA, 3D HAADF-STEM of incomplete dumbbell, magnetic measurements at 300 K, simulated 3D view of the magnetization configuration and simulated hysteresis loops for single Co-Fe dumbbells, 3D animation of the reconstructed HAADF series and the reconstructed volumes of the Fe and Co EDX maps . This material is available free of charge via the Internet at http://pubs.acs.org

AUTHOR INFORMATION

Corresponding Author

*Katerina Soulantica

*e-mail: ksoulant@insa-toulouse.fr

Author Contributions

The manuscript was written through contributions of all authors. All authors have given approval to the final version of the manuscript. The authors declare no competing financial interests

ACKNOWLEDGMENT

The authors thank the ANR for the project “Batmag”, the French national project EMMA (ANR12 BS10 013 01). the European Commission for the FP7 NAMDIATREAM project (EU NMP4-LA-2010-246479), and the METSA network for the HRTEM. This and has received funding from the European Union Seventh Framework Programme under Grant Agreement 312483 - ESTEEM2 (Integrated Infrastructure Initiative–I3). It was also supported by Programme Investissements d'Avenir under the program ANR-11-IDEX-0002-02, reference ANR-10-LABX-0037-NEXT". The authors acknowledge financial support from European Research Council (ERC Advanced Grant # 24691-COUNTATOMS, and ERC Starting Grant # 335078-COLOURATOMS).

ABBREVIATIONS

TEM Transmission Electron Microscopy; HRTEM High Resolution Transmission Electron Microscopy; SQuID Superconducting Quantum interference Device; HDA hexadecylamine; LA lauric acid; XRD X-Ray Diffraction; HAADF-STEM High Angle Annular Dark Field Scanning

Transmission Electron Microscopy; EDX Energy Dispersive X-ray; EELS Electron Energy Loss Spectroscopy; FFT Fast Fourrier Transform; GPA Geometrical Phase Analysis

REFERENCES

(1) Peng, X.; Schlamp, M.C.; Kadavanich, A.; Alivisatos, A.P. *J. Am. Chem. Soc.* **1997**, *119*, 7019-7029.

(2) Li, Y.; Zhang, Q.; Nurmikko, A.V.; Sun, S. *Nano Lett.* **2005**, *5*, 1689-1692.

(3) Costi, R.; Saunders, A.E.; Elmalem, E.; Salant, A.; Banin, U. Visisble *Nano Lett.* **2008**, *8*, 637-641.

(4) Lee, Y.; Garcia M.A.; Frey Huls, N.A.; Sun, S. *Angew. Chem. Int. Ed.* **2010**, *49*, 1271-1274.

(5) Lee, J-S.; Bodnarchuk, M.I.; Shevchenko, E.V.; Talapin, D.V. *J. Am. Chem. Soc.* **2010**, *132*, 6382-6391.

(6) Cozzoli, P.D.; Pellegrino, T.; Manna, L. *Chem. Soc. Rev.* **2006**, *35*, 1195-1208.

(7) Carbone, L.; Cozzoli, P.D. *Nano Today* **2010**, *5*, 449-493.

(8) Costi, R.; Saunders, A.; E.; Banin, U. *Angew. Chem. Int. Ed.* **2010**, *49*, 4878-4897/

(9) Chaudhuri, R. G.; Paria, S. *Chem. Rev*. **1012**, *112*, 2373-2433.

(10) Wang, C.; Xu, C.; Zeng, H.; Sun, S. *Adv. Mater*. **2009**, *21*, 3045-3052.

(11) Pellegrino, T.; Fiore, A.; Carlino, E.; Giannini, C.; Cozzoli, P. D.; Ciccarella, G.; Respaud, M.; Palmirotta, L.; Cingolani, R.; Manna, L. *J. Am. Chem. Soc.* **2006,** *128*, 6690-6698.

(12) Salant, A.; Amitay- Sadovsky, E.; Banin, U. *J. Am. Chem. Soc.* **2006**, *128*, 10006-10007.

(13) Yu, H.; Chen, M.; Rice, P.M.; Wang, S.X.; White, R.L.; Sun, S. *Nano Lett*. **2005**, *5*, 379-382.

(14) Milliron, D.J.; Hughes, S.M.; Cui, Y.; Manna, L.; Li, J.; Wang, L-W.; Alivisatos, A.P. *Nature* **2004**, *430*, 190-195.

(15) Mokari, T.; Rothenberg, E.; Popov, I.; Costi, R.; Banin, U. *Science* **2004**, *304*, 1787-1789.

(16) Vaneski, A.; Sushe, A.S.; Rodriguez-Fernandez, J.; Berr, M.; Jäckel, F.; Feldmann, J.; Rogach, A.L. *Adv. Funct. Mater.* **2011**, *21*, 1547-1556.

(17) Banin, U.; Ben-Shahar, Y.; Vinokurov, K. *Chem. Mater*. **2014**, *26*, 97-110.

(18) Camargo, P.H.; Xiong, Y.; Ji, L.; Zuo, J.M.; Xia, Y. *J. Am. Chem. Soc.* **2007**, *129*, 15452-15453.

(19) Mao, J.; Cao, X.; Zhen, J.; Shao, H.; Gu, H.; Lu, J.; Ying, J.Y. *J. Mater. Chem*. **2011**, *21*, 11478-11481.

(20) Grzelczak, M.; Pérez-Juste, J.; Rodriguez-Gonzalez B.; Liz-Marzan, L.M. *J. Mater. Chem.* **2006**, *16*, 3946-3951.

(21) Habas, S. E.; Lee, H.; Radmilovic, V.; Somorjai, G. A. ; Yang, P. *Nature Materials* **2007**, *6*, 692-697.

(22) Dumestre, F.; Chaudret, B.; Amiens C.; Respaud, M.; Renaud, P.; Zurcher, P. *Angew. Chem., Int. Ed.* **2003**, *42*, 5213-5216.

(23) Wetz, F.; Soulantica, K.; Respaud, M.; Falqui, A.; Chaudret, B. *Mater. Sci. Eng., C* **2007**, *27*, 1162-1166.

(24) Soulantica, K.; Wetz, F.; Maynadié, J.; Falqui, A.; Tan, R. P.; Blon, T.; Chaudret, B.; Respaud, M. *Appl. Phys. Lett*. **2009**, *95*, 152504.

(25) Wetz, F.; Soulantica K.; Falqui A.; Respaud M.; Snoeck E.; Chaudret B. *Angew. Chem*. *Int. Ed*. **2007**, *46*, 7079-7081.

(26) Maynadié, J.; Salant, A.; Falqui, A.; Respaud, M.; Shaviv, E.; Banin, U.; Soulantica, K.; Chaudret B. *Angew. Chem. Int. Ed*., **2009**, *48*, 1814-1817.

(27) Rivest, J. B.; Swisher, S. L.; Fong, L-K.; Alivisatos, A. P. *ACS Nano*, **2011**, *5*, 3811–3816.

(28) Kneller, E. F.; Hawig, R. *IEEE Trans. Mag*, **1991**, *27(4),* 3588–3600.

(29) Skomski, R.; Coey, J. M. D. *Phys. Rev. B* **1993**, *48*, 15812-15816.

(30) Schrefl, T.; Kronmüller, H.; Fidler, J. *J. Magn. Magn. Mater*. **1993**, *127*, L273-L277.

(31) Zeng, H; Li, J.; Liu, J.P.;Wang, Z.L.; Sun, S. *Nature* **2002**, *420*, 395-398.

(32) Calderone, V. R.; Shiju, N. R;. Curulla-Ferr, D.; Chambrey, S.; Khodakov, A.; Rose, A.; Thiessen, J.; Jess, A.; Rothenberg, G. *Angew.Chem. Int. Ed*. **2013**, *52*, 4297-4401. (33) Liu, J-X.; Su, H-Y.; Sun, D-P.; Zhang, B-Y.; Li, W-X. *J. Am. Chem. Soc.* **2013**, *135*, 16284-16287.

(34) Lacroix, L.-M.; Lachaize, S.; Falqui, A.; Respaud, M.; Chaudret, B. *J. Am. Chem. Soc.* **2009**, *131*, 549–557.

(35) Van Tendeloo, G.; Bals, S.; Van Aert, S.; Verbeeck, J.; Van Dyck, D. *Advanced Materials*, **2011**, *24*, 5655-5675.

(36) Bals, S.; Casavola, M.; Van Huis, M.; Van Aert, S.; Batenburg, K. J.; Van Tendeloo, G; Vanmaekelbergh, D., *Nano Letters*, **2011**, *11*, 3420-3424.

(37) Goris, B.; Bals, S.; Van den Broek,W.; Carb¢-Argibay,E.; G¢mez-Grana,S.; Liz-Marzán,M.; Van Tendeloo,G. *Nature Materials*, **2012**, *11*, 930-935.

(38) Goris, B.; De Backer,A.; Van Aert,S.; Gomez-Grana,S.; Liz-Marz n,L.M.; Van Tendeloo,G.; Bals,S. *Nano Letters*, **2013**, *13*, 4236 – 4241.

(39) Midgley, P.A.; Weyland, M. *Ultramicroscopy*, **2003**, *96*, 413-431.

(40) Möbus, G.; Inkson, B.J. *Materials Today* **2007**, *10*, 18-25.

(41) Co [uvtw] (hkil) // Fe [u'v'w'] (h'k'l') means that the Co (hkil) plane is parallel to the Fe (h'k'l') plane and that for these planes the Co [uvtw] direction is parallel to the Fe [u'v'w'] direction.

(42) Schlicke, H.; Ghosh, D.; Fong, L-K.; Xin, H.L.; Zheng, H.; Alivisatos, A.P. *Angew. Chem. Int. Ed*., **2013**, *52*, 980-982.

(43) Hÿtch, M. J.; Snoeck, E.; Kilaas, R. *Ultramicroscopy* **1998**, *74*, 131–146.

(44) Hÿtch, M. J.; Putaux, J.-L.; Pénisson, J.-M. *Nature* **2003**, *423*, 270–273.

(45) Randle, V. "The role of the coincidence site lattice in grain boundary engineering", Woodhead Publishing Limited, Cambridge, UK, 1997.

(46) Liakakos, N. *et al. J. Am. Chem. Soc* **2012**. *134*, 17922-17931.

(47) Snoeck E. ; Gatel, C.; Lacroix, L. M.; Blon, T.; Lachaize, S.; Carrey J.; Respaud, M.; Chaudret B. *Nano Lett.*, **2008**, *8*, 4293–4298.

(48) Ung, D.; Soumare, Y.; Chakroune, N.; Viau, G.; Vaulay, M.-J.; Richard, V.; Fiévet, F. *Chem. Mater*. **2007**, *19*, 2084–2094.

(49) Lacroix L-M. Thesis dissertation, **2008**, INSA, Toulouse.

(50) Donahue M. J. ; Porter D. G. 1999 *OOMMF User's Guide, Version 1.0, Interagency Report* NISTIR 6376, National Institute of Standards and Technology, Gaithersburg, MD.

(51) Astinchap, B.; Moradian, R.; Ardu, A.; Cannas, C.; Varvaro, G.; Capobianchi, A. *Chem. Mater.* **2012**, *24*, 3393-3400.

(52) Ceylan, S ; Friese, C ; Lammel, C ; Mazac, K ; Kirschning, A. *Angew. Chem. Int. Ed.* **2008**, *47*, 8950 –8953

Figure for Table of Contents